Acta Cryst. (1998). A**54**, 806–819

Diffraction Physics

A. Authier* and C. Malgrange

Laboratoire de Minéralogie Cristallographie, Universités P. et M. Curie et D. Diderot, associées au CNRS, Case 115, 4 Place Jussieu, 75252 Paris CEDEX 05, France. E-mail: authier@lmcp.jussieu.fr

(*Received 26 May 1998; accepted 26 August 1998*)

Abstract

The main theories of diffraction are briefly described and their more important results compared. The limitations of the geometrical theory are discussed and the concept of extinction introduced. The main features of the diffraction by a perfect crystal are briefly reviewed: total reflection and Darwin width associated with the Bragg gap, standing waves, anomalous absorption, ray tracing, plane-wave and spherical-wave *Pendellösung*, polarization properties. Real crystals are seldom perfect. They may be nearly perfect with small strains and/or individual lattice defects faults or they may be highly deformed with large strains and a high density of defects. The diffraction by the former is handled using extensions of the dynamical theory of diffraction by perfect crystals using ray tracing. The results are analytical in the case of a constant strain gradient and are otherwise described by simulations which can be compared to the experimental results. The latter case is more difficult but can be approached by more sophisticated theories such as that of Takagi and Taupin.

André Authier studied at the University of Paris and at the Ecole Normale Supérieure. He obtained a DSci from the University of Paris in 1961 and was Professor at the University of Paris (now Université P. et M. Curie) from 1965 to 1996. He became Professor Emeritus in 1997. He was the first President of the European Crystallographic Committee (now European Crystallographic Association) from 1972 to 1975. He was President of the International Union of Crystallography from 1990 to 1993. He is Editor of Section A of Acta Crystallographica and of Volume D of International Tables for Crystallography.

Cecile Malgrange studied at the University of Paris and at the Ecole Normale Supérieure. She entered the CNRS in 1962 and defended her thesis (thèse d'Etat) in 1967. At that time she became Maitre de Conférences at the Faculté des Sciences de Paris and since 1978 she has been Professor at Université Paris 7 - Denis Diderot.

1. Introduction

Diffraction of waves by crystals has permitted the development of crystallography in the 20th century. It all started with Ewald's thesis and his theory of reflection and refraction, which relates the macroscopic properties of dispersion and refraction in a crystal to the interaction of the propagating waves with a microscopic distribution of resonators, that is with its atomic structure. The derivation does not depend on the wavelength and it is this remark by him in January 1912 in answer to a question by Laue that started off Laue's reasoning and led to Friedrich & Knipping's decisive experiment. It was promptly followed by Laue's geometrical theory and Darwin's geometrical and dynamical theories (Darwin, 1914*a*,*b*). Ewald's extension of his theory to the case of X-rays (Ewald, 1916, 1917) shows that refraction and reflection of light waves and X-ray diffraction are essentially the same physical phenomenon.

The scope of diffraction physics is very wide, ranging from the interaction of waves with matter to diffraction theory for perfect and imperfect crystals, powders, modulated structures, paracrystals *etc.*, extinction theory, X-ray optics, interferometry, imaging of defects, ... and only limited aspects will be broached upon in this paper.

2. The theories of diffraction

2.1. *Geometrical theory*

The basis of Laue's 'geometrical theory' of X-ray diffraction is given in the very first of the two papers that gave the account of the discovery of X-ray diffraction (Friedrich *et al.*, 1912): the amplitude diffracted by a three-dimensional periodic assembly of atoms is derived by adding the amplitudes of the waves diffracted by each atom, simply taking into account the optical path differences between them, but neglecting the interaction of the propagating waves and matter. This can be expressed simply using Fourier transforms. The expression of the distribution of electronic density (or more generally of diffracting centres) of a triply periodic infinite medium, $\rho_\infty(\mathbf{r})$, can be written as the convolution of the electron density in one cell, $\rho_0(\mathbf{r})$, by a triply

ISSN 0108-7673

periodic distribution of Dirac distributions located at the nodes of the direct lattice. In practice, the crystal is not infinite, but limited in space and, if $y(\mathbf{r})$ is a shape function equal to 1 inside the medium and 0 outside, the electronic density of the crystal is

$$\rho(\mathbf{r}) = \rho_\infty(\mathbf{r})y(\mathbf{r}) \quad \text{with} \quad \rho_\infty(\mathbf{r}) = \rho_o(\mathbf{r}) * \sum_{i=-\infty}^{\infty} \delta(\mathbf{r} - \mathbf{r}_i), \tag{1}$$

where $\mathbf{r}_i = u_i\mathbf{a} + v_i\mathbf{b} + w_i\mathbf{c}$ is the position vector of the origin of a cell (u_i, v_i and w_i integers).

According to the geometrical theory, the total scattered amplitude is the sum of the amplitudes scattered by each diffracting centre, simply taking into account their optical path differences. If we assume a continuous distribution of diffracting centres, $\rho(\mathbf{r})\,\mathrm{d}\tau$, the distribution of diffracted amplitude is given in reciprocal space by

$$\mathcal{A}(\mathbf{\Delta K}) = \int \rho(\mathbf{r}) \exp(-2\pi i \mathbf{\Delta K} \cdot \mathbf{r})\,\mathrm{d}\tau, \tag{2}$$

where the integration is over the whole volume of the diffracting medium, $\mathbf{\Delta K} = \mathbf{K_h} - \mathbf{K_o}$ is the diffraction vector (Fig. 1) and the amplitude diffracted by a diffraction centre is taken to be unity. Substituting the expression for $\rho(\mathbf{r})$, and noticing that, since $y(\mathbf{r})$ is 0 outside the crystal, the limits of integration can be taken as infinite, the expression for $\mathcal{A}(\mathbf{\Delta K})$ is seen to be a Fourier transform. Using the properties of Fourier transforms, it follows that

$$\mathcal{A}(\mathbf{\Delta K}) = V^{-1} \sum_{\mathbf{h}} F_{hkl} Y(\mathbf{\Delta K} - \mathbf{h}), \tag{3}$$

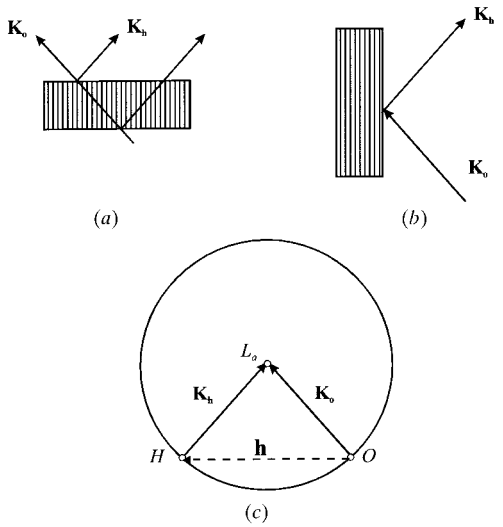

Fig. 1. Diffraction according to the geometrical theory. (*a*) Direct space, Laue geometry; (*b*) direct space, Bragg geometry; (*c*) reciprocal space. $\mathbf{OH} = \mathbf{h}$: reciprocal-lattice vector; L_a: Laue point (centre of the Ewald sphere); $\mathbf{OL_a} = \mathbf{K_o}$: incident wave ($OL_a = k$); $\mathbf{HL_a} = \mathbf{K_h}$: reflected wave ($HL_a = k$); these both satisfy the Bragg condition.

where V is the volume of the unit cell, the sum is over all reciprocal-lattice vectors $\mathbf{h}$,

$$F_{hkl} = \int_{-\infty}^{\infty} \rho_o(\mathbf{r}) \exp(2\pi i \mathbf{h} \cdot \mathbf{r})\,\mathrm{d}\tau$$

is the usual structure factor and $Y(\mathbf{\Delta K})$ is the Fourier transform of the shape function, $\mathcal{F}[y(\mathbf{r})]$. This expression shows that the scattered amplitude is distributed around each reciprocal-lattice point and that it is given by the Fourier transform of the shape function, weighted by the structure factor. This result calls for a certain number of remarks:

(i) The fine structure of each diffraction spot depends only on the size and shape of the crystal.

(ii) The diffracted amplitude does not depend on the reaction of matter on the wave; this is because geometrical theory assumes that the amplitude incident on every diffracting centre is the same; this assumption can only be expected to be valid when the interaction is very weak and this point will be further discussed below.

(iii) $Y(\mathbf{\Delta K} - \mathbf{h})$ is proportional to the volume of the crystal and the scattered amplitude increases to infinity when the crystal increases towards infinity. This is not physically possible because it violates the conservation of energy and is due to the assumption just recalled (Darwin, 1914*b*).

(iv) The expression for the intensity depends on the shape of the crystal. It is, in reflection geometry, for a plane-parallel plate and for unpolarized radiation (see, for instance, James, 1950):

$$I_h = \frac{R^2\lambda^2(1 + \cos^2 2\theta)}{2\sin^2\theta} V^2 |F_{hkl}|^2 \left[\frac{\sin(2\pi kt \cos\theta\Delta\theta)}{2\pi kt \cos\theta\Delta\theta}\right]^2,$$

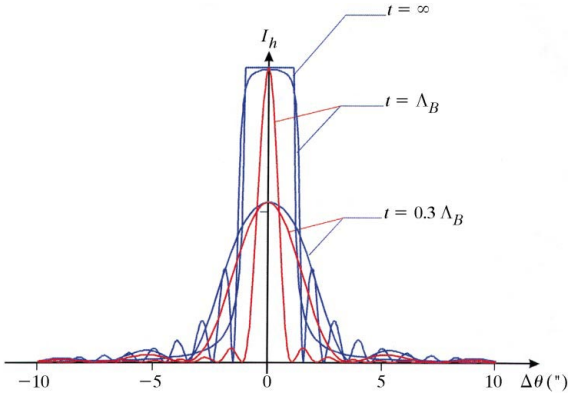

Fig. 2. Comparison of the rocking curves according to the dynamical and the geometrical theory, reflection geometry; silicon, Mo $K\alpha$, 220, assuming zero absorption. Blue curves: dynamical theory with $t = 0.3\Lambda_B$, Λ_B, ∞, respectively ($\Lambda_B = 6.82$ µm); red curves: geometrical theory, with $t = 0.3\Lambda_B$ and Λ_B, respectively, normalized and centred at the same angular position as the corresponding curve given by dynamical theory; for $t = \infty$, the geometrical theory gives a Dirac distribution.

where $\Delta\theta$ is the difference between the incident angle and the Bragg angle and R is the classical radius of the electron. Its full width at half-maximum (FWHM) is $\delta_{\rm geom} = 0.44295\lambda/t\cos\theta$. Its maximum and the integrated intensity under the rocking curve are proportional to the square of the structure factor. The rocking curve is represented in Fig. 2 for two different crystal thicknesses (for comparison purposes with dynamical theory, these thicknesses are given in terms of a parameter, Λ_B, defined in the next section).

If the crystal is very large, the diffracted intensity is concentrated at the reciprocal-lattice points and the diffraction geometry is as is represented in Fig. 1: there is reflection for one incident wavevector only, $\mathbf{OL_a} = \mathbf{K_o}$, which satisfies Bragg's law, where L_a is the centre of the Ewald sphere passing through the reciprocal-lattice points O and H.

2.2. *Darwin's dynamical theory*

In the second of his fundamental papers, Darwin (1914*b*) took into account the interaction between the lattice planes and the propagating waves: at each lattice plane, the incident wave is both reflected and transmitted; each of the waves just generated is in turn reflected and transmitted each time it crosses a lattice plane. Darwin showed that the balance of transmitted and reflected amplitudes can be described at each lattice plane by recurrence equations. By solving this set of equations, it is possible to obtain the expression of the amplitue reflected at the surface of the crystal. If the crystal is semi-infinite (of infinite thickness) and not absorbing, one finds that, for a very narrow angular range at the centre of the reflection domain, this amplitude is pure imaginary. The corresponding reflected intensity is equal to 1, this is the total reflection domain; the rocking curve presents the famous top-hat shape (Fig. 2). Its angular width is proportional to the structure factor and so is the integrated intensity. The theory was extended to the case of absorbing crystals by Prins (1930), who showed that there is no longer a total reflection domain. When the crystal thickness is finite, there is also no longer total reflection even for a non-absorbing crystal (Fig. 2) and, when the thickness becomes very small, the expression for the integrated intensity, I_{hi}(dyn.), tends towards that obtained with the geometrical theory, I_{hi}(geom.). It is, for a symmetrical reflection:

$$I_{hi}(\text{dyn.}) = I_{hi}(\text{geom.})\frac{\tanh(\pi t/\Lambda_B)}{\pi t/\Lambda_B}, \qquad (4a)$$

where t is the crystal thickness and

$$\Lambda_B = \frac{\pi V \sin\theta}{R\lambda|C|(F_{hkl}F_{\bar{h}\bar{k}\bar{l}})^{1/2}} \qquad (4b)$$

is called the extinction distance; $|C| = 1$ or $\cos 2\theta$ for σ (normal to the diffraction plane) and π polarization (parallel to the diffraction plane), respectively, $F_{\bar{h}\bar{k}\bar{l}}$ is the structure factor associated with the $\bar{h}\bar{k}\bar{l}$ reflection.

The coefficient $\tanh(\pi t/\Lambda_B)/(\pi t/\Lambda_B)$ tends towards 1 when t/Λ_B tends towards zero. For instance, it is equal to 0.968, 0.992 and 0.999 for $t/\Lambda_B = 0.1$, 0.05 and 0.01, respectively. This shows that, for the approximation of the geometrical theory to be better than 3%, the crystal thickness must be smaller than one tenth of the extinction distance. For a given crystal thickness, the longer the extinction distance, the better the geometrical theory approximation is.

Darwin's work had been limited to the reflection geometry but it was adapted to the transmission geometry by Borie (1967).

2.3. *Extinction*

Darwin (1914*a*,*b*) compared the intensities calculated with his dynamical theory with the experimental measurements by Moseley & Darwin (1913) on rock salt and found them in profound disagreement both with respect to the value of the reflected intensity and with respect to the width of the reflection domain which was very much larger than predicted. He was so certain of his theoretical derivation that he concluded that this disagreement was certainly due to the imperfections of the crystal. This led him to develop his model of *extinction* and of diffraction by a crystalline conglomerate (Darwin, 1922). This model was further refined by Bragg *et al.* (1926) with the concept of the *mosaic* crystal. They considered that real crystals are made of a mosaic of small blocks more or less misoriented with respect to one another. The geometrical theory applies to the very thin blocks only. When their thickness is larger, their reflectivity becomes closer to that predicted by the dynamical theory and a correction must be applied, which is given by equation (4*a*); this is the *primary extinction*. The incident beam crosses many blocks. If their misalignment is larger than the width of the rocking curve of the individual blocks, they reflect different fractions of the incident beam and the total intensity is the sum of the intensities reflected by the blocks. But if two successive blocks are nearly parallel, part of the incident intensity is reflected off by the first block before it reaches the second one. This is the origin of the *secondary-extinction* correction, which is taken into account by an artificial absorption correction. If the crystal is made of a mosaic of widely misoriented very thin crystals, the geometrical theory applies and the crystal is said to be *ideally imperfect*. This model is of course very crude and in general does not correspond physically to the nature of the imperfections in crystals. It was improved by Hamilton (1957) and by Zachariasen (1967, 1968) who introduced energy-transfer equations to take into account the coupling between the beams transmitted and diffracted by successive blocks. They involve both the mosaic spread between the blocks and

the size of the blocks. The model was further refined by Becker & Coppens (1974, 1975), whose formalism is well adapted to many experimental results (Palmer & Jauch, 1995). A comparison of the extinction theories based on the Darwin mosaic model is given in Sabine (1988).

Another and more modern approach has been used by different authors. It is based on the Takagi–Taupin equations which generalize the fundamental equations of the dynamical theory for any kind of wave and allow for deformations of the crystalline lattice (see §4.2); these equations are amplitude-transfer equations. Different theories may be mentioned, such as Kato's statistical theory (Kato, 1991, 1994) and Kulda's random elastic deformation theory (Kulda, 1987, 1991). Reviews and comparison with experiment are given in Schneider *et al.* (1992) and in Takama & Harima (1994).

2.4. *Ewald's and Laue's dynamical theory*

One of main results of Ewald's dynamical theory is the rediscovery of the total-reflection domain. But it has a much wider scope than Darwin's and it was far ahead of its time. Of utmost importance is the introduction of the notion of wavefields (Ewald, 1913). The optical field that propagates through the crystal and excites the dipoles is a sum of plane waves, called the *wavefield*, whose wavevectors can be deduced from one another by translations in reciprocal space:

$$\mathbf{E} = \mathbf{E_o}\exp(-2\pi i\mathbf{K_o}\cdot\mathbf{r}) + \mathbf{E_h}\exp(-2\pi i\mathbf{K_h}\cdot\mathbf{r}) + \mathbf{E_g}\exp(-2\pi i\mathbf{K_g}\cdot\mathbf{r}) + \ldots \quad (5)$$

with $\mathbf{K_h} = \mathbf{K_o} + \mathbf{h}$, $\mathbf{K_g} = \mathbf{K_o} + \mathbf{g}$, where $\mathbf{h} = \mathbf{OH}$ and $\mathbf{g} = \mathbf{OG}$ are reciprocal-lattice vectors (Fig. 3 – only two reciprocal-lattice points, *O* and *H*, are represented). The *Bloch wave* introduced much later by Bloch in the theory of electrons in solids (Bloch, 1928) corresponds to exactly the same notion. The wavefield is characterized by its tiepoint, which is the common extremity of the wavevectors, $\mathbf{K_o} = \mathbf{OP}$, $\mathbf{K_h} = \mathbf{HP}$, $\mathbf{K_g} = \mathbf{GP}$ *etc.*

In contrast to Ewald's theory which discusses the interaction of an electromagnetic wave with a distribution of discrete dipoles, von Laue's basic assumption (von Laue, 1931, 1960) is to consider that the electric negative and positive charges are distributed in a continuous way throughout the volume of the crystal. Since the crystal must be neutral, they cancel out and the local electric charge and density of current are equal to zero. The electric field, **E**, the electric displacement, **D**, the magnetic field, **H**, and the magnetic induction, **B**, are related by Maxwell's equations and by the material relations that describe the reaction of the medium to the electromagnetic field:

$$\mathbf{D} = \varepsilon\mathbf{E} = \varepsilon_0(1+\chi)\mathbf{E} \quad (6)$$
$$\mathbf{B} = \mu\mathbf{H},$$

where ε and μ are the dielectric constant and the magnetic permeability of the medium, respectively, ε_0 the dielectric constant of vacuum and χ the electric susceptibility or polarizability of the medium. The magnetic interaction of X-rays with the electron distribution is very small and is neglected in classical dynamical theory; μ is then simply replaced by μ_0, magnetic permeability of vacuum. This interaction was, however, observed as early as 1972 using a conventional X-ray tube (de Bergevin & Brunel, 1972), but is now studied with synchrotron radiation (for a review, see Lovesey & Collins, 1996).

The polarizability is classically shown to be proportional to the electronic density and is therefore triply periodic. The key point of the dynamical theory is the dispersion equation. From both Ewald's and Laue's formulations, it can be shown that the amplitude of any one wave can be expressed in terms of the amplitudes of all the waves in the wavefield with the following relation:

$$\mathbf{E_h} = [K_\mathbf{h}^2/(K_\mathbf{h}^2 - k^2)]\sum_{\mathbf{h}'}\chi_{\mathbf{h}'}\mathbf{E}_{\mathbf{h}'[\mathbf{h}]}, \quad (7)$$

where $\chi_\mathbf{h} = -R\lambda^2|C|F_{hkl}/(\pi V)$ is the Fourier coefficient of the polarizability, $k = 1/\lambda$, $\mathbf{E}_{\mathbf{h}'[\mathbf{h}]}$ is the projection of $\mathbf{E}_{\mathbf{h}'}$ on the plane normal to the wavevector $\mathbf{K_h}$.

This is a set of linear equations. Its solution is nontrivial if the associated determinant is zero. The corresponding secular equation is the *dispersion equation*. Each equation (7) contains a sum over an infinite number of terms. The factors $K_\mathbf{h}^2/(K_\mathbf{h}^2 - k^2)$, called resonance factors by Ewald, are, however, only non-negligible when the wavenumber $K_\mathbf{h}$ is very close to the wave number in vacuum, *k*. If only one term is non-negligible, then only one wave propagates in the medium, with wavenumber *nk* (*n* is the index of refraction); the extremity of the wavevector lies on a sphere of centre *O* and radius *nk*. If there are two, two waves propagate, with wavevectors $\mathbf{OP} = \mathbf{K_o}$ and $\mathbf{HP} = \mathbf{K_h}$ (Fig. 3) and there are two reciprocal-lattice nodes lying very close to the Ewald sphere. This is the most frequently studied case but the situation when there are more terms (the *n*-beam case) is also very

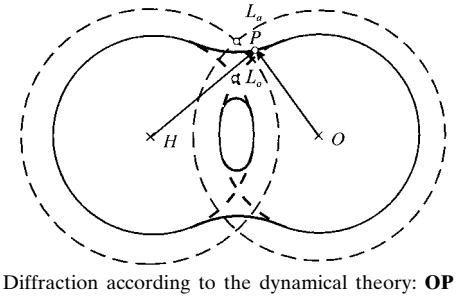

Fig. 3. Diffraction according to the dynamical theory: $\mathbf{OP} = \mathbf{K_o}$ and $\mathbf{HP} = \mathbf{K_h}$ are the wave vectors inside the crystal. Solid curve: dispersion surface; *P*: tiepoint. L_a: Laue point; $OL_a = k$: wavenumber in vacuum; L_o: Lorentz point; $OL_o = nk$: wavenumber in the crystal (*n* is the index of refraction).

interesting and is discussed in the paper by Chang (1998) in this issue.

The dispersion equation relates the lengths of the wavevectors of the various waves in the wavefield, $K_{\mathbf{o}}$, $K_{\mathbf{h}}$ *etc.*; it is the equation of the locus of the tiepoint, *P*, which is a connecting surface between the spheres centred at *O*, *H etc.* and of radii *nk*, called dispersion surface. It is represented schematically on Figs. 3 and 4 in the two-beam case. The main properties of the dispersion surface are the following:

(i) The dispersion surface is a surface of revolution around **OH** and its intersection with the diffraction plane, $\mathbf{K_o}$, $\mathbf{K_h}$ is a hyperbola whose asymptotes are the tangents to the sphere of centres *O* and *H* and of radii *nk*; it has two branches, labelled 1 and 2, branch 1 being on the same side as the Laue point (Fig. 4).

(ii) The dispersion surface is analogous to the band diagram in the theory of solids; the former is a constant energy surface and the latter represents the variations of the energy with position in reciprocal space, but they proceed from a similar derivation. The separation between the branches of the dispersion surface is equivalent to the gap between two successive bands and the diameter

$$G_B = \overline{A_{o2}A_{o1}} = \frac{R\lambda|C|(F_{hkl}F_{\bar{h}\bar{k}\bar{l}})^{1/2}}{\pi V \cos\theta} \qquad (8a)$$

of the dispersion surface is sometimes called for that reason *Bragg gap*; it is larger, the larger the structure factor is, that is the stronger the interaction of the waves with matter, and the longer is the wavelength. Its inverse, Λ_L, is the *Pendellösung* distance in the symmetric Laue case and is related to the extinction distance defined for the Bragg case (4*b*) by:

$$\Lambda_L = G_B^{-1} = \Lambda_B \cot\theta. \qquad (8b)$$

(iii) The propagation direction of a wavefield, indicated by the Poynting vector, **S**, is along the normal to the dispersion surface at the tiepoint.

(iv) An incident plane wave excites in the crystal two wavefields whose tiepoints are obtained by applying boundary conditions on the wavevectors at the entrance surface. In the transmission geometry or Laue case (Fig. 1*a*), their tiepoints lie, one on branch 1 and the other one on branch 2; as the crystal is rocked through the reflection domain, both branches of the dispersion surface are therefore excited simultaneously. In the reflection geometry or Bragg case (Fig. 1*b*), the tiepoints of the two wavefields lie on the same branch of the dispersion surface. One of them is not physically meaningful if the crystal is very thick, but both of them are for a thin crystal, one of the wavefields being back-reflected at the bottom surface of the crystal. As the crystal is rocked through the reflection domain one goes through three zones: in the first one, the tiepoint(s) lie(s) on one branch of the dispersion surface; in the second one, the tiepoint(s) lie(s) within the Bragg gap and is(are) imaginary; and in the third one the tiepoint(s) lie(s) on the second branch. If the crystal is very thick, there is total reflection when the physically meaningful tiepoint lies within the Bragg gap. The angular width of the domain of total reflection is therefore proportional to the Bragg gap. If the crystal is thin and two wavefields are excited, these interfere, giving rise to the oscillations in the rocking curves which can be seen in Fig. 2 (equal-orientation *Pendellösung* fringes).

(v) Expression (8*a*) for the Bragg gap is proportional to the polarization factor $|C| = 1$ or $\cos 2\theta$ for σ and π polarization, respectively, and this shows that there are two sheets of the dispersion surface according to the polarization (Fig. 4). The index of refraction is therefore different according to the direction of polarization and this is the equivalent of birefringence in optics. An incident plane-polarized wave will generate in the crystal two coherent waves propagating with different velocities which combine to produce an elliptically polarized wave. This is true even far from the centre of the reflection domain and is used to produce phase plates (Giles *et al.*, 1994; Malgrange, 1996).

(vi) The width of the total reflection domain or Darwin width is

$$\delta_{\rm dyn} = \frac{\lambda|\gamma|^{1/2}}{\Lambda_B \cos\theta} = \frac{|\gamma|^{1/2}G_B}{k\sin\theta} = 2d_{hkl}|\gamma|^{1/2}G_B, \qquad (9)$$

where γ is a geometrical factor depending on the asymmetry of the reflection and d_{hkl} is the distance between reflecting planes. It is proportional to the Bragg gap, very small, of the order of a few seconds of arc and is smaller, the smaller the structure factor and the smaller the wavelength; it is also strongly dependent on

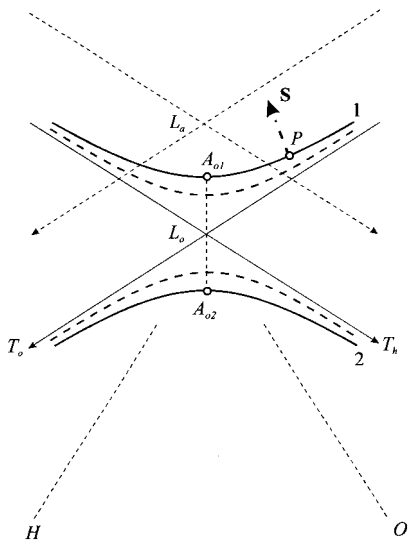

Fig. 4. Dispersion surface. *P*: tiepoint of a wavefield. **S**: Poynting vector of that wavefield; A_{o1}, A_{o2}: vertices of the dispersion surface. Solid line: σ polarization ($C = 1$); dashed line: π polarization ($C = \cos 2\theta$).

the asymmetry of the reflection and by combining various reflections on several crystals (cut or not from the same monolithic block) it is possible to produce beams of any width and shape; this is the basis of X-ray optics for synchrotron radiation described by Hart & Berman (1998) in this issue.

The main features of the diffraction by a perfect crystal are described in §3.

2.5. *Comparison between the results of the geometrical and the dynamical theories*

In practice, the only useful information provided by the geometrical theory is the diffracted intensity. From the shape of the rocking curve (its width, its asymmetry), information can be deduced relative to the particle size, the distribution of twin and stacking faults, order–disorder in the distribution of atomic positions (for a review, see Warren, 1969). For structure determination, it is the integrated intensity that is useful.

It is interesting to compare the results of the geometrical and dynamical theories. In Fig. 2, rocking curves are compared according to the two theories in reflection geometry for a perfect crystal of increasing thickness. It can be seen that they become identical for values of the crystal thickness that are a fraction of Λ_B (between 1/10 and 1/3, according to how accurate one wishes to be) but, as the crystal thickness increases towards infinity, the FWHM of the rocking curve according to the geometrical theory tends towards 0 while that of the rocking curve according to the dynamical theory saturates at a value equal to the Darwin width.

A similar comparison can be performed for the integrated intensity. It is given by (4*a*) in reflection geometry. In the Laue case, and for a nonabsorbing case, the integrated intensity has been calculated by von Laue (1960) using dynamical theory:

$$I_{hi} = \frac{R\lambda^2 |C\chi_{\mathbf{h}}| (F_{hkl}F_{\bar{h}\bar{k}\bar{l}})^{1/2}}{2V \sin 2\theta} \int_0^{2\pi t \Lambda_L^{-1}} J_0(z)\, \mathrm{d}z,$$

where $J_0(z)$ is the zeroth-order Bessel function.

When the ratio of the crystal thickness to the *Pendellösung* distance, $t/\Lambda_L = tG_B$, tends towards zero, this expression tends towards

$$I_{hi} = \frac{R\lambda^2 |C| (F_{hkl}F_{\bar{h}\bar{k}\bar{l}})^{1/2}}{2V \sin 2\theta} 2\pi t \Lambda_L^{-1} = \frac{R^2\lambda^3 C^2 |F_{hkl}F_{\bar{h}\bar{k}\bar{l}}| t}{V^2 \cos\theta \sin 2\theta},$$

which is identical to the expression obtained with the geometrical theory. Fig. 5 compares the variations of the integrated intensity obtained with the two theories.

Equation (4*a*) and Figs. 2 and 5 show that the approximation of the geometrical theory is more and more satisfactory as the Bragg gap (8*a*) decreases. The inverse of the Bragg gap is a length in direct space that can be considered as a yardstick with which one can determine whether the reflected intensity according to the geometrical theory is a good approximation. By varying the diffraction conditions, one varies the length of this yardstick and, for a given thickness, the primary-extinction correction.

The importance of the inverse of the Bragg gap, Λ_L, as a yardstick can be readily understood by remembering that, in the geometrical theory, there is only one position for the tiepoint: the Laue point (Fig. 1); if one takes refraction into account, then it would be the Lorentz point, L_o (Fig. 3). As the Bragg gap tends towards zero, the two vertices of the dispersion surface, A_{o1} and A_{o2} (Fig. 4), tend towards each other until the dispersion surface is reduced to the Lorentz point. This can be achieved either by reducing the interaction (going to higher-order reflections or to neutrons instead of X-rays) or by going towards high energies (small wavelengths). The geometrical theory corresponds therefore to a situation where the crystal does not react on the waves, and is what Ewald called an *empty* crystal.

Example. The fact that the 'apparent' perfection of a crystal depends on the conditions of diffraction is illustrated, for instance, by the following experience by Freund (1990). He studied the variation with wavelength of the integrated intensity of the 222 reflection of several copper crystals with different degrees of perfection: samples B_1 to B_4 were Bridgman crystals with dislocation densities 2×10^4, 4×10^4, 7×10^4 and 2×10^7 dislocations cm^{-2}, repectively, and sample C_1 was a dislocation-free Czochralski crystal (Fig. 6). The wavelength ranged from 0.03 to 1.66 Å. Sample C_1 behaves like a perfect crystal for wavelengths greater than 0.1 Å but seems quite imperfect for wavelengths smaller than about 0.07 Å. Samples B_1, B_2 and B_3 behave almost like a perfect crystal for wavelengths above the *K*-absorption edge of copper, whereas for a wavelength of about 0.01 Å they behave like an ideal mosaic crystal, with every intermediary stage in between. Sample B_4 behaves essentially like a mosaic crystal. These results can be interpreted with the remark of the preceding paragraph. As the wavelength and the diameter $\overline{A_{o2}A_{o1}}$ of the dispersion surface becomes shorter, the length of the yardstick increases and the

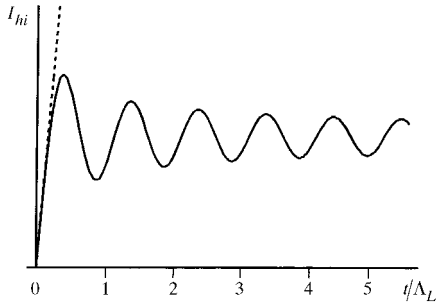

Fig. 5. Variations of the integrated intensity with crystal thickness in the transmission case and zero absorption. Solid line: dynamical theory; dashed line: geometrical theory.

'coherent' domains in the samples appear smaller and smaller: the samples behave more and more like ideally imperfect crystals.

3. Diffraction by a perfect crystal

The diffraction properties of waves by crystals result from the properties of the wavefields. If the notion of wavefield was introduced by Ewald who predicted their elementary properties, their physical existence was proved experimentally much later, through three decisive observations: anomalous absorption, *Pendellösung* and double refraction.

3.1. *Standing waves – anomalous absorption*

The intensity of the wavefield described by (5) is, in the most usual two-beam case

$$|\mathbf{E}|^2 = |\mathbf{E_o}|^2 + |\mathbf{E_h}|^2 + 2|\mathbf{E_o}\mathbf{E_h}| \cos 2\pi(\mathbf{h}\cdot\mathbf{r} + \Psi), \tag{10}$$

where Ψ is the phase associated with $E_\mathbf{h}/E_\mathbf{o}$. von Laue noted that this expression shows that the two waves interfere and produce a set of standing waves. The term $\cos 2\pi(\mathbf{h}\cdot\mathbf{r} + \Psi)$ expresses that the nodes lie on planes parallel to the lattice planes and that their periodicity is equal to the distance $1/h = d_{hkl}$, where $d_{hkl} = d/n$, d is the lattice plane spacing and n the order of the reflection. If the origin is taken on an atomic plane, the phase Ψ is equal to π for wavefields associated with branch 1 of the dispersion surface and equal to 0 for wavefields associated with branch 2 of the dispersion surface. The nodes of standing waves therefore lie on the atomic planes for a wavefield associated with branch 1 of the dispersion surface while it is the antinodes (maxima of electric feld) that lie on the atomic planes for wavefields associated with the other branch of the dispersion surface (Fig. 7). Borrmann pointed out that the former would undergo a very small absorption and penetrate through thick crystals while the latter would be absorbed out very rapidly. This is the phenomenon of anomalous absorption, or Borrmann effect, discovered by Borrmann (1941, 1950) and calculated by von Laue (1949). The anomalous-absorption effect is maximum at the centre of the reflection domain: the tiepoint of the wavefield with a minimum absorption coefficient is A_{o1} and the tiepoint of the wavefield with a maximum absorption coefficient is A_{o2}. For instance, for a germanium crystal and Mo $K\alpha$ radiation, the normal absorption coefficient is $\mu_o = 320\,\mathrm{cm}^{-1}$ and the minimum effective absorption coefficient is $\mu_{\min} = 11.5\,\mathrm{cm}^{-1}$ (Ludewig, 1969).

It has been noted in §2.4 that the dispersion surface has different sheets for the two directions of polarization. The theory shows that the coefficient of anomalous absorption is also different. It is therefore possible to make an X-ray polarizer by using a sufficiently thick crystal (Cole *et al.*, 1961).

A very interesting and now very developed application of the standing waves formed by wavefields was proposed by Batterman (1964, 1969): in the Bragg case, as one rocks the crystal through the reflection domain, the tiepoints lie first on branch 1 and then on branch 2; the phase Ψ varies by π, and the system of nodes and antinodes glides by half a lattice plane distance inside the crystal. When an antinode of an electric field passes through an atom, there is a high absorption as has been noted and, therefore, emission of X-ray fluorescence and photoelectrons. If this emission is recorded simultaneously with the angular position of the crystal, the position of the atom within the unit cell along the normal to the reflecting plane can be measured. This effect, which was first observed by Golovchenko *et al.*

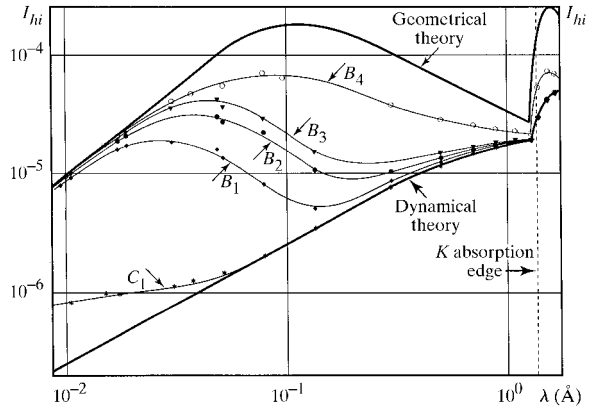

Fig. 6. Variations with wavelength of the integrated intensity of the 222 reflection from several copper crystals of different degrees of perfection; samples B_1 to B_4 are Bridgman crystals with dislocation densities 2×10^4, 4×10^4, 7×10^4 and 2×10^7 dislocations cm^{-2}, repectively, and sample C_1 is a dislocation-free Czochralski crystal; the markers represent the experimental values, the thick solid lines represent the theoretical values for the mosaic and the perfect crystal, respectively (after Freund, 1990).

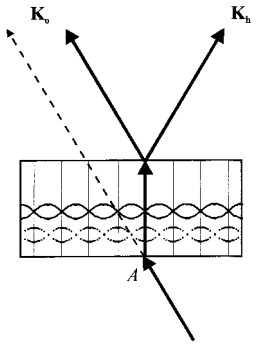

Fig. 7. Borrmann effect: the standing-wave nodes lie on the atomic planes for branch 1 of the dispersion surface (full lines). The corresponding wavefields undergo small absorption. For branch 2, the antinodes lie on the atomic planes (dotted lines) and there is a high absorption. In a thick absorbing crystal, the path of the wavefields is along the lattice planes.

(1974), is used to record the position of impurities at crystal surfaces and interfaces and to study the sructure of surfaces and interfaces (for reviews, see Bedzyk, 1988; Malgrange & Ferret, 1992; Zegenhagen, 1993; Lagomarsino, 1996; Patel, 1996).

3.2. *Spherical waves – Pendellösung*

In the two-beam case, the incident wave generates two wavefields inside the crystal whose reflected waves are: $\mathbf{E_{h1}}\exp(-2\pi i\mathbf{K_{h1}}\cdot\mathbf{r})$ and $\mathbf{E_{h2}}\exp(-2\pi i\mathbf{K_{h2}}\cdot\mathbf{r})$. In the regions where they overlap, they interfere and the resulting intensity is

$$|\mathbf{E_{h1}}|^2+|\mathbf{E_{h2}}|^2+2|\mathbf{E_{h1}}||\mathbf{E_{h2}}|\cos[2\pi(\mathbf{K_{h1}}-\mathbf{K_{h2}})\cdot\mathbf{r}+\varphi],$$

where φ is the phase difference between $|\mathbf{E_{h1}}|$ and $|\mathbf{E_{h2}}|$.

There is thus a periodic variation of the intensity of the reflected wave as was shown by Ewald (1917) and which he called the oscillating solution, or *Pendellösung*, of the dynamical theory. If P_1 and P_2 are the tiepoints of the two wavefields, the period of the oscillations is

$$\Lambda=\overline{P_2P_1}^{-1}=|\mathbf{K_{h1}}-\mathbf{K_{h2}}|^{-1}.$$

For instance, in the Laue symmetrical case, in the middle of the reflection domain, the two tiepoints are A_{02} and A_{01} (Fig. 4) and the period is the *Pendellösung* distance, Λ_L [equation (8*b*)].

The *Pendellösung* oscillations were only observed 42 years after Ewald's prediction, by Kato & Lang (1959) and in a slightly different context. They observed equal-thickness fringes on projection topographs (Lang, 1959) along the edges of a wedge-shaped silicon crystal which Kato interpreted as *Pendellösung* fringes due to the interferences of wavefields produced by a spherical wave. Ewald's (and Laue's) theory had been derived in the case of an incident plane wave but such a wave is not produced naturally for X-rays. In those pre-synchrotron days, X-rays were produced as spherical waves by X-ray tubes. The dynamical theory was extended to incident spherical waves by Kato for both nonabsorbing (Kato, 1960, 1961) and absorbing crystals (Kato, 1968).

Pendellösung fringes were later observed in the rocking curves of thin crystals using a pseudo-plane wave as incident beam. These observations were made both in the reflection geometry (Batterman & Hildebrandt, 1968) and in the transmission geometry (Lefeld-Sosnowska & Malgrange, 1969).

The precise measurement of the period of *Pendellösung* fringes has been used by a number of authors to determine with high accuracy the structure factor of very perfect crystals such as quartz, germanium and silicon (see, for instance, Yamamoto *et al.*, 1968; Hart & Milne, 1969; Kato, 1969; Bonse & Teworte, 1980; Deutsch & Hart, 1985; Graf & Schneider, 1986; Saka & Kato, 1986).

3.3. *Ray tracing: Borrmann triangle, double refraction of X-rays*

It was mentioned in §2.4 that one of the important properties of the wavefields is that their direction of propagation, given by the Poynting vector, is along the normal to the dispersion surface (von Laue, 1952). For an incident plane wave that, by definition, has an infinite lateral extension, this is difficult to check. Real waves, whichever way they have been produced or conditioned by optical systems, always have a certain divergence and, in dealing with their propagation, one has to reason with wavepackets. It is well known in optics that in a dispersive medium the direction of propagation of the energy of a wavepacket is along the normal to the surfaces of indices. For X-ray diffraction, the dispersion surface plays the same role and the direction of propagation is indeed along the normal to the dispersion surface (Ewald, 1958; Wagner, 1959). If the divergence of the incident beam is wider than the angular width of the reflection domain, the whole dispersion surface is excited and there is a whole fan of wavefield trajectories within the triangle of angle 2θ between the incident and the reflected directions as is shown in Fig. 8 in transmission geometry: this is the Borrmann fan, or Borrmann triangle (Borrmann, 1959). A very important consequence is the phenomenon of *angular* amplification: while the angular width of the fan of wavevectors exciting the whole dispersion surface is of a few seconds of arc only, that of the fan of the corresponding trajectories is of several degrees (twice the Bragg angle). This amplification ratio applies to any wavepacket within the Borrmann triangle: if $\delta\theta$ is the angular width of the corresponding wavevectors, the angular width $\delta\alpha$ of the associated trajectories is $\delta\alpha=\mathcal{A}\delta\theta$. The value of this amplification ratio, $\mathcal{A}$, depends on the position of the tiepoint on the dispersion surface and varies from 10^4 or more at the centre of the dispersion surface to 1 far from the reflection domain.

Two methods were used in the early days to isolate wavepackets and to determine their direction of propagation. The first one is due to Borrmann. It was

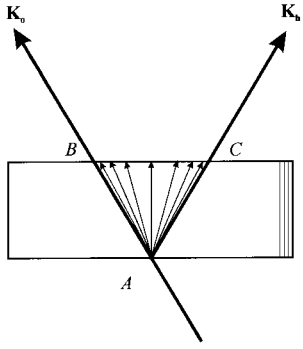

Fig. 8. Borrmann triangle; $\mathbf{K_o}$: incident direction; $\mathbf{K_h}$: reflected direction.

mentioned in §3.1 that anomalous absorption is most important for the wavefields whose tiepoints are at the vertices of the dispersion surface, A_{02} and A_{01}. Their propagation direction is along the normal to the dispersion surface, which, for these points, is parallel to the lattice planes. For a very high value of $\mu_o t$ (t crystal thickness) out of the whole Borrmann fan, the only wavefields that will go through the crystal are those whose tiepoints are very close to A_{01} and whose direction of propagation is nearly parallel to the lattice planes (Fig. 7). The crystal then acts as a waveguide. This observation by Borrmann (1954) was a direct proof of the existence of the wavefields as a physical reality and not merely as a mathematical concept.

The second method consisted in the observation by Authier (1960) of the double refraction predicted by Borrmann (1955, 1959). It was noted in §2.4 that an incident plane wave excites four wavefields inside the crystal, two for each direction of polarization; this is what Borrmann called *Vierfachbrechung*. The paths of the wavefields corresponding to the two directions of polarization are too close to be separated but it is possible to observe a double refraction. In the experiment by Authier (1960), a double-crystal setting was used (Fig. 9). The first crystal is thick and not too absorbing. A slit S enables a narrow wavepacket to be isolated from the beam coming out of the base B_1C_1 of the Borrmann triangle of this first crystal. Owing to the angular amplification, the divergence of this wavepacket is very much smaller than the width of the rocking curve and it can be considered as a pseudo-plane wave. It is incident on a second crystal of the same material (silicon), set for the same Bragg reflection. It excites two wavefields with different paths in this second crystal and, because the lateral expansion of the wavepacket is sufficiently small, the paths can be separated on a photographic plate placed outside the exit surface of the crystal. By rocking the crystal slightly, the angle of incidence of the wavepacket could be varied and therefore also the paths of the wavefields excited in the second crystal. It was thus possible to confirm the physical reality of the wavefields and to trace their paths in the crystal (*ray tracing*). The same method was used for the first observation of plane-wave *Pendellösung* fringes (Malgrange & Authier, 1965). The beam coming from the slit is incident on a thick wedge-shaped crystal; where the second crystal is thin enough, the paths of the two wavefields overlap and *Pendellösung* fringes are observed, while, where the crystal is thicker, the paths of the wavefields separate and no fringes are observed (Fig. 10).

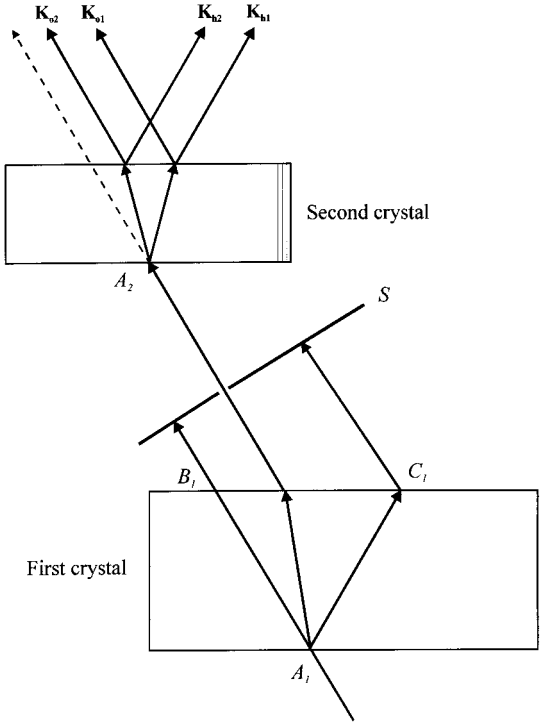

Fig. 9. Double refraction. $\mathbf{K}_{o1}$, $\mathbf{K}_{h1}$: wavevectors of wavefield 1; $\mathbf{K}_{o2}$, $\mathbf{K}_{h2}$: wavevectors of wavefield 2; S: slit.

3.4. *Applications of dynamical diffraction by perfect crystals*

Several applications of dynamical diffraction have already been mentioned: accurate determination of structure factors using measurement of *Pendellösung* fringes, standing-wave studies of the structure of surfaces and interfaces and of the adsorption of impurities at surfaces and interfaces, design of polarizers and of phase plates. Other applications are described in the papers by Chang (1998) and by Hart & Berman (1998) in this Special Issue.

Another very interesting application is the X-ray interferometer developed by Bonse & Hart (1965). It has many applications, such as phase-contrast microscopy, measurement of lattice parameters on an absolute scale, determination of the Avogadro number or,

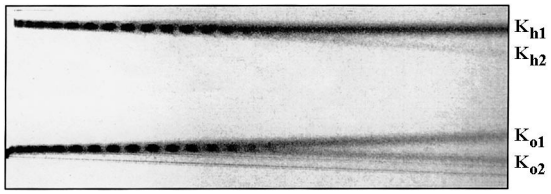

Fig. 10. Plane-wave *Pendellösung* fringes. The second crystal in the setting of Fig. 9 is wedge-shaped; where it is thin enough, the paths of the two wavefields overlap and interference fringes are produced; where it is thicker, the paths separate and there are no longer fringes. $\mathbf{K}_{o1}$, $\mathbf{K}_{o2}$ indicate the traces of the refracted beams for branch 1 and branch 2 wavefields, respectively; $\mathbf{K}_{h1}$, $\mathbf{K}_{h2}$ indicate the traces of the reflected beams for branch 1 and branch 2 wavefields, respectively (after Malgrange & Authier, 1965).

conversely, measurement of displacements on a nanometre scale, the 'Ångström ruler' (Hart, 1968), measurement of very minute strains *etc.* For an introduction to the principles of X-ray and neutron interferometers, see Colella (1996), and for a review of their design and applications, see Bowen (1996).

4. Diffraction by imperfect crystals

Since the early days when the calculated diffracted intensities were first compared with experimental values, it was realised that most crystals contain imperfections, some being nearly perfect, such as calcite and quartz, the others more or less highly imperfect. It was not until silicon and germanium were grown for their applications as semiconductors that crystals of a high degree of perfection were obtained. For structure-determination purposes, it is usually better to use crystals imperfect enough for the geometrical theory to be applicable and the extinction corrections to be negligible. If this is not the case for some of the more intense reflections, it is necessary to have a good model for the extinction corrections or to go to high-energy X-rays where these corrections will be less important. But for many applications of crystals as high-technology materials, good-quality crystals must be used and it is usually necessary to characterize the nature and the distribution of defects. For this purpose, one must develop extensions of the diffraction theory for imperfect crystals. One may distinguish three cases:

(i) The crystal is only slightly deformed (regime I). The notions of dispersion surface and of wavefields as they were defined in §§2.4 and 3 are still valid. The paths of the wavefields in the deformed materials are bent as are rays of light in a region of varying index of refraction (the mirage effect); the variations of reflected intensity are calculated using 'ray theories' based on the traditional dynamical theory (§4.1).

(ii) The crystal is strongly deformed, but there is a model to describe the distribution of strain (regime II). When the strain gradient becomes very large, the divergence of wavepackets increases, as in light optics, because diffraction effects occur (in the optical sense of the term); this is accompanied for X-rays by 'interbranch scattering' (creation of new wavefields on the opposite branch of the dispersion surface) and the ray theories are no longer valid. New forms of the dynamical theories, such as those developed by Takagi (1962, 1969) and Taupin (1964) must be used; their principle is briefly described in §4.2. If one applies a strain gradient to a perfect crystal and increases it, passing progressively through regimes I and II, one may span the whole domain of variations of intensities, from the values given by the perfect-crystal dynamical theory to the values given by geometrical theory for the 'ideally imperfect' crystal; the strain distribution may be determined by comparison between theory and experiment.

(iii) The crystal is strongly deformed but the distribution of defects is so complicated that it cannot be modelled: statistical dynamical theories must be used.

4.1. *Ray tracing in slightly deformed crystals*

It is well known in light optics that, if a wavepacket propagates in a region where the index of refraction n varies, the direction of the main vector of the wavepacket varies accordingly. Its variation

$$\delta\mathbf{k} \sim \overrightarrow{\nabla n} \tag{11}$$

ensures the continuity of the tangential component of the wavevector as the beam crosses regions of different indices of refraction. The direction of propagation of the wavepacket is along the normal to the surface of indices and can be found by applying Fermat's principle.

Penning & Polder (1961) made the hypothesis that when the deformation of the crystal is small enough it is possible to consider at each point a local perfect crystal, *asymptotic* to the real deformed one to which dynamical theory applies.

Local strain in a deformed crystal is due partly to a rotation of the lattice planes and partly to a variation of the lattice parameter. The path of the wavefields inside the crystal and their intensity are determined by the local variation of their departure from Bragg's angle, called *effective misorientation*, $\delta\theta$. It can be expressed in reciprocal space (Authier, 1966):

$$\delta\theta = -\delta\mathbf{h} \cdot \mathbf{s}_\mathbf{h}/k \sin 2\theta \tag{12}$$

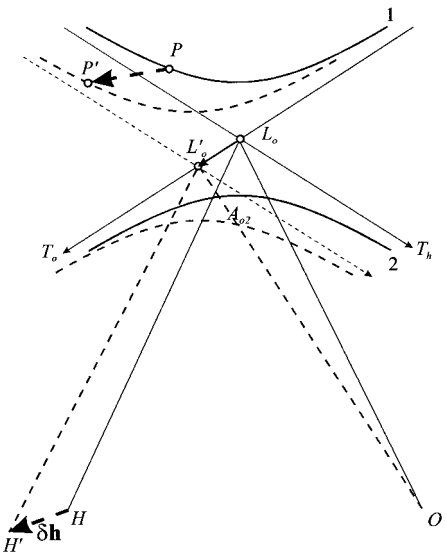

Fig. 11. Ray theory. The dispersion surface after a deformation is represented by dotted lines. *P*: tiepoint before deformation; *P*′: tiepoint after deformation; $\delta\mathbf{h}$: variation of the reciprocal-lattice vector.

where $\mathbf{s_h}$ is a unit vector in the reflected direction and

$$\delta\mathbf{h} = -\nabla[\mathbf{h}\cdot\mathbf{u}(\mathbf{r})] \tag{13}$$

is the local variation of the reciprocal-lattice vector; $\mathbf{u}(\mathbf{r})$ is the local displacement field associated with the strain.

To a first approximation, the structure factor and therefore also the diameter of the dispersion surface are not affected by the deformation. As the Lorentz point necessarily lies on a sphere centred at the origin O of the reciprocal space, which is invariant, and with radius nk, that is, in practice, on its tangential plane T_o, the effect of the deformation is simply to translate the dispersion surface along T_o, the shift being $L_o\vec{L}'_o = nk\delta\theta$ (Fig. 11). The position of the tiepoint on the dispersion surface varies and so does the direction of propagation of the wavefield which is still given by that of the normal to the dispersion surface. The path of the wavefield in the crystal is obtained as in light optics by applying Fermat's principle (Penning & Polder, 1961; Kato, 1963, 1964). This is the so-called *Eikonal approximation* (Kato, 1963).

The variation of the local wavevector is

$$\delta\mathbf{K_o} = \mathbf{OP}' - \mathbf{OP} = \mathbf{PP}'.$$

Equation (12) shows that the dispersion surface is invariant if $\delta\mathbf{h}\cdot\mathbf{s_h} = 0$. The surfaces $\delta\mathbf{h}\cdot\mathbf{s_h} =$ constant can therefore be interpreted as surfaces of constant index of refraction and, by analogy to (11), the local variation of the wavevector is

$$\delta\mathbf{K_o} \sim \vec{\nabla}(\delta\mathbf{h}\cdot\mathbf{K_h}). \tag{14}$$

The parameter that is used in the derivation of the ray trajectories is actually proportional to $\delta\mathbf{K_o}\cdot\mathbf{s_o}$, where $\mathbf{s_o}$ is a unit vector in the incident direction. It is given by

$$\beta = -\frac{\Lambda_L}{\cos^2\theta}\delta\mathbf{K_o}\cdot\mathbf{s_o} = \frac{\Lambda_L}{\cos^2\theta}\frac{\partial^2(\mathbf{h}\cdot\mathbf{u})}{\partial s_o \partial s_h},$$

after substitution of (13) into (14), and is called the *strain gradient*. One can note here that, for a given distortion, β is larger, the larger the yardstick, Λ_L, mentioned in §2.5 is (the inverse of the Bragg gap).

It is usually more convenient to consider the dispersion surface as invariant and the reciprocal-lattice points as mobile relative to it. The tiepoint is then displaced along the dispersion surface. A simple case is that where the strain gradient β is constant, which can be obtained by a pure mechanical bending of the lattice planes, a temperature gradient or a concentration gradient. The paths of the wavefields are then sections of hyperbolae, as shown in Fig. 12, drawn in the case of an incident spherical wave and in transmission geometry. It can be seen in the figure that, at any point p of the base of the Borrmann triangle, BC, two wavefields arrive, one excited on branch 1 of the dispersion surface (solid line) and one excited on branch 2 (dotted line). They interfere, giving rise to equal-strain *Pendellösung* fringes on X-ray diffraction topographs (Kato, 1964; Patel & Kato, 1973).

4.2. *Takagi–Taupin theory*

The theory developed by Takagi (1962, 1969) and Taupin (1964) constitutes a generalization of the dynamical theory for any kind of incident wave and any kind of deformation. Its principle is to consider the crystal wave as a modified Ewald wave which can be developed as a sum of *modulated* waves:

$$\mathbf{E} = \sum_{\mathbf{h}} \mathbf{E_h}(\mathbf{r})\exp(-2\pi i\mathbf{K_h}\cdot\mathbf{r}) \tag{15}$$

with $\mathbf{K_h} = \mathbf{K_o} - \mathbf{h}$. The amplitudes $\mathbf{E_h}(\mathbf{r})$ of the constituting waves are slowly varying functions of the position vector $\mathbf{r}$ and wavevector $\mathbf{K_o}$ has an arbitrary orientation, chosen at will, and is of length nk. The local variations of the phases are thus included in those of the amplitudes. The hypothesis that $\mathbf{E_h}(\mathbf{r})$ is a slowly varying function implies that $\boldsymbol{\Delta}[\mathbf{E_h}(\mathbf{r})]$ can be neglected, which is not true for very large deformations.

The consequence of the fact that the amplitudes are now modulated is that the set of linear equations (7) is replaced by a set of partial differential equations that can be written, in the two-beam case:

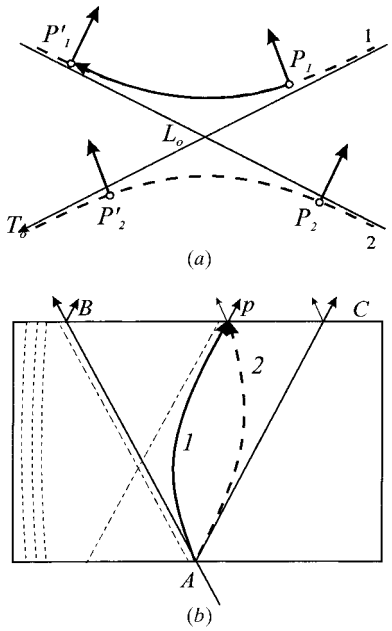

Fig. 12. Ray trajectories in a crystal with a constant strain gradient β. (*a*) Reciprocal space: as the wavefield propagates in the strained crystal, its tiepoint is displaced from P_1 to P'_1. (*b*) Direct space: the path of a wavefield is a hyperbola whose curvature is in the same sense as that of the lattice planes for branch 1 (solid line), its asymptotes are thin broken lines; the path of a wavefield belonging to branch 2 is represented as a thick dotted line; the lattice planes are represented as thin dotted lines.

$$\left.\begin{aligned}\partial E_{\mathbf{o}}(\mathbf{r})/\partial s_{\mathbf{o}} &= -i\pi k C\chi'_{\bar{\mathbf{h}}}(\mathbf{r})E_{\mathbf{h}}(\mathbf{r})\\ \partial E_{\mathbf{h}}(\mathbf{r})/\partial s_{\mathbf{h}} &= -i\pi k C\chi'_{\mathbf{h}}(\mathbf{r})E_{\mathbf{o}}(\mathbf{r})\end{aligned}\right\} \quad (16)$$

where $\chi'_{\mathbf{h}} = \chi_{\mathbf{h}} \exp[2\pi i\mathbf{h}\cdot\mathbf{u}(\mathbf{r})]$ is the Fourier coefficient of the expansion of the polarizability of the deformed crystal and $\mathbf{K}_{\mathbf{o}}$ has been chosen equal to $\mathbf{OL}_{\mathbf{o}}$.

In some simple cases such as a perfect crystal and an incident plane or spherical wave or a constant strain gradient, it is possible to find an analytical solution to (16). Otherwise, it is necessary to calculate numerical solutions with a computer (Authier *et al.*, 1968; Epelboin, 1983). It is possible in this way to simulate the images of defects on X-ray diffraction topographs (for a review, see Epelboin, 1985) or to similate the rocking-curve profiles for crystals with surface layers or epilayers (see, for instance, Halliwell *et al.*, 1984; Fewster, 1992) or with implanted layers (for a review, see Servidori, Cembali & Milita, 1996).

The Takagi–Taupin theory has also been used to interpret the phenomenon of 'interbranch scattering' mentioned in the introduction to this section. Authier & Balibar (1970) showed that ray theory is only valid when the variation of the effective misorientation over a *Pendellösung* distance is much less than the width of the rocking curve; when this is not the case, new wavefields are created on the other branch of the dispersion surface. Balibar *et al.* (1975), by solving Takagi–Taupin equations numerically, showed that the generation of new wavefields occurs when the strain gradient β is larger than a critical value $\beta_c = \pi/(2\Lambda_L)$ and when the wavefield trajectories are paralllel to the lattice planes (Fig. 13). Balibar *et al.* (1983) for the Laue case and Chukhovskii & Malgrange (1989) for the Bragg case confirmed this result analytically and showed that the fraction of the intensity that is transferred to the new wavefield is $\exp(-2\pi\beta_c/\beta)$. This was also shown numerically by Gronkowski & Malgrange (1984) in the case of a variable-strain gradient. These results enable the ray theory to be extended to highly deformed crystals and to give in some cases a quantitative interpretation of their rocking curves.

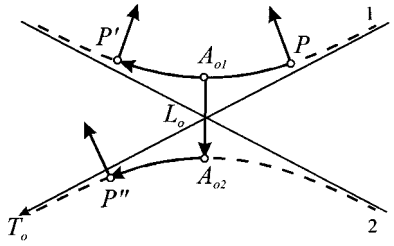

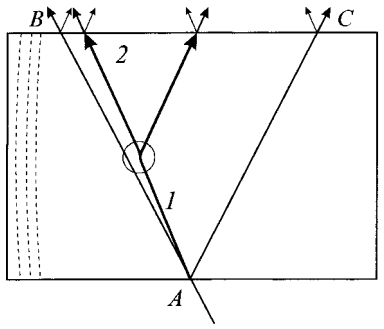

Fig. 13. Interbranch scattering when the strain gradient β is very large. (*a*) Reciprocal space: a new wavefield is excited on the other branch of the dispersion surface when the tiepoint reaches A_{o1}. (*b*) Direct space: the path of the new wavefield is labelled 2.

5. Concluding remarks

The development of diffraction physics can be roughly divided into three major stages. In the first one, which lasted up to the early 1940s, the bases of diffraction theories were laid down: the diffracted intensities were calculated according to the geometrical and dynamical theories and extinction was invoked to interpret intensities measured from real crystals. In the second one, which lasted up to the early 1960s, on one hand properties related to the propagation of X-rays in perfect crystals were observed for the first time, a number of them predicted by Ewald – wavefields, anomalous absorption, *Pendellösung* – and, on the other hand, the bases of diffraction theories by imperfect crystals were developed. The third stage, corresponding to modern times, has seen very big steps forward: the results of the studies in these two directions have led to many applications of practical importance, X-ray optics for synchrotron radiation, qualitative and quantitative characterization of crystal imperfections by imaging and diffractometry techniques, combined with computer simulations; the Takagi–Taupin and the statistical dynamical theories make it possible to bridge the gap between the 'perfect' and the 'ideally imperfect' crystal and to understand how the transition takes place.

References

Authier, A. (1960). *C. R. Acad. Sci.* **251**, 2003–2005.
Authier, A. (1966). *J. Phys. (Paris)*, **27**, 57–60.
Authier, A. & Balibar, F. (1970). *Acta Cryst.* A**26**, 647–654.
Authier, A., Malgrange, C. & Tournarie, M. (1968). *Acta Cryst.* A**24**, 126–136.
Balibar, F., Chukhovskii, F. N. & Malgrange, C. (1983). *Acta Cryst.* A**39**, 387–399.
Balibar, F., Epelboin, Y. & Malgrange, C. (1975). *Acta Cryst.* A**31**, 836–840.
Batterman, B. W. (1964). *Phys. Rev. A*, **133**, 759–764.
Batterman, B. W. (1969). *Phys. Rev. Lett.* **22**, 703–705.

Batterman, B. W. & Hildebrandt, G. (1968). *Acta Cryst.* A**24**, 150–157.
Becker, P. J. & Coppens, P. (1974). *Acta Cryst.* A**30**, 129–147, 148–153.
Becker, P. J. & Coppens, P. (1975). *Acta Cryst.* A**31**, 417–425.
Bedzyk, M. J. (1988). *Nucl. Instrum. Methods*, A**266**, 679–683.
Bergevin, F. de & Brunel, M. (1972). *Phys. Lett. A*, **39**, 141–142.
Bloch, F. (1928). *Z. Phys.* **52**, 555.
Bonse, U. & Hart, M. (1965). *Appl. Phys. Lett.* **7**, 238–240.
Bonse, U. & Teworte, R. (1980). *J. Appl. Cryst.* **13**, 410–416.
Borie, B. (1967). *Acta Cryst.* **23**, 210–216.
Borrmann, G. (1941). *Phys. Z.* **42**, 157–162.
Borrmann, G. (1950). *Z. Phys.* **127**, 297–323.
Borrmann, G. (1954). *Z. Kristallogr.* **106**, 109–121.
Borrmann, G. (1955). *Naturwissenschaften*, **42**, 67–68.
Borrmann, G. (1959). *Beitr. Phys. Chem. 20 Jahrhunderts*, pp. 262–282. Braunschweig: Vieweg und Sohn.
Bowen, D. K. (1996). *X-ray and Neutron Dynamical Diffraction: Theory and Applications*, edited by A. Authier, S. Lagomarsino & B. K. Tanner, *NATO ASI Ser., Ser. B: Physics*, No. 357, pp. 381–410. New York/London: Plenum Press.
Bragg, W. L., Darwin, C. G. & James, R. W. (1926). *Philos. Mag.* **1**, 897–922.
Chang, S.-L. (1998). *Acta Cryst.* A**54**, 886–894.
Chukhovskii, F. N. & Malgrange, C. (1989). *Acta Cryst.* A**45**, 732–738.
Cole, H., Chambers, F. W. & Wood, C. G. (1961). *J. Appl. Phys.* **32**, 1942–1945.
Colella, R. (1996). *X-ray and Neutron Dynamical Diffraction: Theory and Applications*, edited by A. Authier, S. Lagomarsino & B. K. Tanner, *NATO ASI Ser., Ser. B: Physics*, No. 357, pp. 369–380. New York/London: Plenum Press.
Darwin, C. G. (1914*a*). *Philos. Mag.* **27**, 315–333.
Darwin, C. G. (1914*b*). *Philos. Mag.* **27**, 675–690.
Darwin, C. G. (1922). *Philos. Mag.* **43**, 800–829.
Deutsch, M. & Hart, M. (1985). *Acta Cryst.* A**41**, 48–55.
Epelboin, Y. (1983). *Acta Cryst.* A**39**, 761–767.
Epelboin, Y. (1985). *Mater. Sci. Eng.* **73**, 1–43.
Ewald, P. P. (1913). *Phys. Z.* **14**, 465–472.
Ewald, P. P. (1916). *Ann. Phys. (Leipzig)*, **49**, 1–38, 117–143.
Ewald, P. P. (1917). *Ann. Phys. (Leipzig)*, **54**, 519–597.
Ewald, P. P. (1958). *Acta Cryst.* **11**, 888–891.
Fewster, P. F. (1992). *J. Appl. Cryst.* **25**, 714–723.
Freund, A. (1990). *SPIE Conference on Advanced X-ray-UV Radiation Sources and Applications*, *SPIE Proc.* **1345**, 234–244.
Friedrich, W., Knipping, P. & von Laue, M. (1912). *Sitzungsber. K. Bayer. Akad. Wiss.* pp. 303–322 [reprinted in *Ann. Phys. (Leipzig)*, (1913), **41**, 971–990].
Giles, C., Malgrange, C., Goulon, J., de Bergevin, F., Vettier, C., Dartyge, E., Fontaine, A., Giorgetti, C. & Pizzini, S. (1994). *J. Appl. Cryst.* **27**, 232–240.
Golovchenko, J. A., Batterman, B. W. & Brown, W. L. (1974). *Phys. Rev. B*, **10**, 4239–4243.
Graf, H. A. & Schneider, J. R. (1986). *Phys. Rev. B*, **34**, 8629–8638.
Gronkowski, J. & Malgrange, C. (1984). *Acta Cryst.* A**40**, 515–522.
Halliwell, M. A. G., Lyons, M. H. & Hill, M. J. (1984). *J. Cryst. Growth*, **68**, 523–531.
Hamilton, W. C. (1957). *Acta Cryst.* **10**, 629–634.
Hart, M. (1968). *Br. J. Appl. Phys.* **1**, 1405–1408.
Hart, M. & Berman, L. (1998). *Acta Cryst.* A**54**, 850–858.
Hart, M. & Milne, A. D. (1969). *Acta Cryst.* A**25**, 134–138.
James, R. W. (1950). *The Optical Principles of the Diffraction of X-rays.* London: G. Bell and Sons.
Kato, N. (1960). *Z. Naturforsch. Teil A*, **15**, 369–370.
Kato, N. (1961). *Acta Cryst.* **14**, 526–532, 627–636.
Kato, N. (1963). *J. Phys. Soc. Jpn*, **18**, 1785–1791.
Kato, N. (1964). *J. Phys. Soc. Jpn*, **19**, 67–77, 971–985.
Kato, N. (1968). *J. Appl. Phys.* **39**, 2225–2230, 2231–2237.
Kato, N. (1969). *Acta Cryst.* A**25**, 119–128.
Kato, N. (1991). *Acta Cryst.* A**47**, 1–11.
Kato, N. (1994). *Acta Cryst.* A**50**, 17–22.
Kato, N. & Lang, A. R. (1959). *Acta Cryst.* **12**, 787–794.
Kulda, J. (1987). *Acta Cryst.* A**43**, 167–173.
Kulda, J. (1991). *Acta Cryst* A**47**, 775–779.
Lagomarsino, S. (1996). *X-ray and Neutron Dynamical Diffraction: Theory and Applications*, edited by A. Authier, S. Lagomarsino & B. K. Tanner, *NATO ASI Ser., Ser. B: Physics*, No. 357, pp. 225–234. New York/London: Plenum Press.
Lang, A. R. (1959). *J. Appl. Phys.* **30**, 1748–1755.
Laue, M. von (1931). *Ergeb. Exakten Naturwiss.* **10**, 133–158.
Laue, M. von (1949). *Acta Cryst.* **2**, 106–113.
Laue, M. von (1952). *Acta Cryst.* **5**, 619–625.
Laue, M. von (1960). *Röntgenstrahl-Interferenzen.* Frankfurt am Main: Akademische Verlagsgesellschaft.
Lefeld-Sosnowska, M. & Malgrange, C. (1969). *Phys. Status Solidi*, **34**, 635–647.
Lovesey, S. W. & Collins, S. P. (1996). *X-ray Scattering and Absorption by Magnetic Materials. Oxford Series on Synchrotron Radiation.* Oxford: Clarendon Press.
Ludewig, J. (1969). *Acta Cryst.* A**25**, 116–118.
Malgrange, C. (1996). *X-ray and Neutron Dynamical Diffraction: Theory and Applications*, edited by A. Authier, S. Lagomarsino & B. K. Tanner, *NATO ASI Ser., Ser. B: Physics*, No. 357, pp. 91–109. New York/London: Plenum Press.
Malgrange, C. & Authier, A. (1965). *C. R. Acad. Sci.* **261**, 3774–3777.
Malgrange, C. & Ferret, D. (1992). *Nucl. Instrum. Methods Phys. Res.* A**314**, 285–296.
Moseley, H. G. J. & Darwin, C. G. (1913). *Philos. Mag.* **26**, 210.
Palmer, A. & Jauch, W. (1995). *Acta Cryst.* A**51**, 662–667.
Patel, J. R. (1996). *X-ray and Neutron Dynamical Diffraction: Theory and Applications*, edited by A. Authier, S. Lagomarsino & B. K. Tanner, *NATO ASI Ser., Ser. B: Physics*, No. 357, pp. 211–224. New York/London: Plenum Press.
Patel, J. R. & Kato, N. (1973). *J. Appl. Phys.* **44**, 971–977.
Penning, P. & Polder, D. (1961). *Philips Res. Rep.* **16**, 419–440.
Prins, J. A. (1930). *Z. Phys.* **63**, 477–493.
Sabine, T. M. (1988). *Acta Cryst.* A**44**, 368–373.
Saka, T. & Kato, N. (1986). *Acta Cryst.* A**42**, 469–478.
Schneider, J. R., Bouchard, R., Graf, H. A. & Nagasawa H. (1992). *Acta Cryst.* A**48**, 804–819.
Servidori, M., Cembali, F. & Milita, S. (1996). *X-ray and Neutron Dynamical Diffraction: Theory and Applications*, edited by A. Authier, S. Lagomarsino and B. K. Tanner, *NATO ASI Ser., Ser. B: Physics*, No. 357, pp. 301–321. New York/London: Plenum Press.

Takagi, S. (1962). *Acta Cryst.* **15**, 1311–1312.
Takagi, S. (1969). *J. Phys. Soc. Jpn*, **26**, 1239–1253.
Takama, T. & Harima, H. (1994). *Acta Cryst.* A**50**, 239–246.
Taupin, D. (1964). *Bull. Soc. Fr. Minéral. Cristallogr.* **87**, 469.
Wagner, E. H. (1959). *Acta Cryst.* **12**, 345–346.
Warren, B. E. (1969). *X-ray Diffraction.* Reading, MA: Addison-Wesley.
Yamamoto, K., Homma, S. & Kato, N. (1968). *Acta Cryst.* A**24**, 232–237.
Zachariasen, W. H. (1967). *Acta Cryst.* **23**, 558–564.
Zachariasen, W. H. (1968). *Acta Cryst.* A**24**, 421–424.
Zegenhagen, J. (1993). *Surf Sci. Rep.* **18**, 199–271.

Acta Crystallographica Section A
Foundations of Crystallography
ISSN 0108-7673

addenda and errata

Nomenclature of magnetic, incommensurate, composition-changed morphotropic, polytype, transient-structural and quasicrystalline phases undergoing phase transitions. II. Report of an IUCr Working Group on Phase Transition Nomenclature. Erratum

J.-C. Tolédano,[a]† R. S. Berry,[b]‡ P. J. Brown,[c] A. M. Glazer,[d] R. Metselaar,[e]§ D. Pandey,[f] J. M. Perez-Mato,[g] R. S. Roth[h] and S. C. Abrahams[i]*¶

[a]Laboratoire des Solides Irradiés and Department of Physics, Ecole Polytechnique, F-91128 Palaiseau CEDEX, France, [b]Department of Chemistry, University of Chicago, 5735 South Ellis Avenue, Chicago, IL 60637, USA, [c]Institut Laue–Langevin, BP 156X CEDEX, F-38042 Grenoble, France, [d]Clarendon Laboratory, University of Oxford, Parks Road, Oxford OXI 3PU, England, [e]Laboratory for Solid State and Materials Chemistry, Eindhoven University of Technology, PO Box 513, NL-5600 MB Eindhoven, The Netherlands, [f]School of Materials Science and Technology, Banaras Hindu University, Varanasi 221005, India, [g]Departamento de Física de la Materia Condensada, Universidad del País Vasco, Apdo 644, E-48080 Bilbao, Spain, [h]B214, Materials Building, National Institute of Standards and Technology, Washington, DC 20234, USA, and [i]Physics Department, Southern Oregon University, Ashland, OR 97520, USA

† Chairman of IUCr Working Group.
‡ *Ex officio*, International Union of Pure and Applied Physics.
§ *Ex officio*, International Union of Pure and Applied Chemistry.
¶ *Ex officio*, IUCr Commission on Crystallographic Nomenclature.

Six printing errors are corrected in the Report by Tolédano *et al.* [*Acta Cryst.* (2001), A**57**, 614–626]. The first is in §2.1, the fourth last sentence of which should read ''Although such nicknames do not always describe the magnetic character of the substance explicitly, since 'AF' for example may be mistaken for antiferroelectric, this lack is compensated for by the fifth and sixth fields (see the examples in §§3.1–3.5).'' The second is in §3.4, second field of the AF phase, which should read '<260 K'. The third is in §4.5, the final sentence of which should be 'However, certain materials display ferroic properties in the incommensurate phase (*cf.* §5.3)'. The fourth is in §5.1, sixth field of phase II, which should read 'Incommensurate. Modulation: $\delta \sim 0.78$. Displacive modulation.'. The fifth is in §6, the third sentence of which should read ''While accepting this definition, it is necessary to point out, however, that the boundary between phases in the examples below need not be 'thermodynamically abrupt' (*i.e.* involve a latent heat and discontinuities in the physical quantities).''. The final error is in §6.1, sixth field of the FT phase, which should read 'FT | $0.45 < x < 1$ | *P*4*mm* (99) | $Z = 1$ | Ferroelectric and ferroelastic | All phases pseudo-cubic perovskites. No perovskite octahedral tilts; 6 variants.'.

References

Tolédano, J.-C., Berry, R. S., Brown, P. J., Glazer, A. M., Metselaar, R., Pandey, D., Perez-Mato, J. M., Roth, R. S. & Abrahams, S. C. (2001). *Acta Cryst.* A**57**, 614–626.

Diffraction physics. Erratum

A. Authier* and C. Malgrange

Laboratoire de Minéralogie Cristallographie, Universités P. et M. Curie et D. Diderot, associé au CNRS, Case 115, 4 Place Jussieu, 75252 Paris CEDEX 05, France

Owing to a copying error, the formula in §2.1(iv) of the paper by Authier & Malgrange [*Acta Cryst.* (1998), A**54**, 806–819] is erroneous and should be replaced by:

$$I_h = \frac{R^2\lambda^2(1+\cos^2 2\theta)}{2\sin^2\theta}\frac{t^2}{V^2}|F_{hkl}|^2\left[\frac{\sin(2\pi kt\cos\theta\Delta\theta)}{(2\pi kt\cos\theta\Delta\theta)}\right]^2.$$

References

Authier, A. & Malgrange, C. (1998). *Acta Cryst.* A**54**, 806–819.

